HHS Public Access

Author manuscript

Ophthalmology. Author manuscript; available in PMC 2016 November 01.

Published in final edited form as:

Ophthalmology. 2015 November ; 122(11): 2316–2326. doi:10.1016/j.ophtha.2015.07.008.

The Onion Sign in neovascular age-related macular degeneration represents cholesterol crystals

Claudine E. Pang, MD[1,2], **Jeffrey D. Messinger, DC**[3], **Emma C. Zanzottera, MD**[3,4], **K. Bailey Freund, MD**[1,2,5], and **Christine A. Curcio, PhD**[3]

[1]Vitreous Retina Macula Consultants of New York, NY

[2]LuEsther T. Mertz Retinal Research Center, Manhattan Eye, Ear, and Throat Institute, New York, NY

[3]Department of Ophthalmology, University of Alabama School of Medicine, Birmingham AL

[4]Eye Clinic, Department of Clinical Science “Luigi Sacco”, Sacco Hospital, University of Milan, Milan, Italy

[5]Department of Ophthalmology, New York University School of Medicine, New York, NY

Abstract

Purpose—To investigate the frequency, natural evolution and histological correlates of layered, hyperreflective, sub-retinal pigment epithelium (sub-RPE) lines, known as the Onion Sign, in neovascular age-related macular degeneration (nvAMD).

Design—Retrospective observational cohort study; an experimental laboratory study.

Participants—Two hundred thirty eyes of 150 consecutive patients with nvAMD; 40 human donor eyes with clinical and histopathologic diagnosis of nvAMD.

Methods—Spectral-domain optical coherence tomography (SD-OCT), near-infrared reflectance (nIR), color fundus images and medical charts were reviewed. Donor eyes underwent multimodal *ex vivo* imaging including SD-OCT before processing for high-resolution histology.

Main Outcome Measures—Presence of layered, hyperreflective sub-RPE lines, qualitative analysis of their change in appearance over time with SD-OCT, histological correlates of these lines, and associated findings within surrounding tissues.

Results—Sixteen of 230 eyes of patients (7.0%) and 2 of 40 donor eyes (5.0%) with nvAMD had layered, hyperreflective sub-RPE lines on SD-OCT imaging. These appeared as refractile,

Corresponding Address: Christine A. Curcio, PhD; Department of Ophthalmology; EyeSight Foundation of Alabama Vision Research Laboratories; 1670 University Boulevard Room 360; University of Alabama School of Medicine; Birmingham AL 35294-0099; Ph 205.996.8682; F 205.934.3425; curcio@uab.edu.

Disclosures: The other authors have no proprietary or commercial interest in any of the materials discussed in this article.

Presentations: Annual meeting of the Association for Research in Vision and Ophthalmology, 2015, Denver CO

yellow-gray exudates on color imaging and hyperreflective lesions on nIR. In all 16 eyes, the Onion Sign persisted in follow-up for up to 5 years, with fluctuations in the abundance of lines and associated with intraretinal hyperreflective foci. Patients with the Onion Sign were disproportionately taking cholesterol-lowering medications ($p = 0.025$). Histology of 2 donor eyes revealed that hyperreflective lines correlated with clefts created by extraction of cholesterol crystals during tissue processing. Fluid surrounding crystals contained lipid yet was distinct from oily drusen. Intraretinal hyperreflective foci correlated with intraretinal RPE and lipid-filled cells of probable monocyte origin.

Conclusion—Persistent and dynamic, the Onion Sign represents sub-RPE cholesterol crystal precipitation in aqueous environment. The frequency of the Onion Sign in nvAMD in a referral practice and a pathology archive is 5–7%. Associations include use of cholesterol-lowering medication and intraretinal hyperreflective foci attributable to RPE cells and lipid-filled cells of monocyte origin.

Keywords

Age-related macular degeneration; neovascularization; retinal pigment epithelium; cholesterol; crystals; optical coherence tomography; histology

Introduction

The Onion Sign was first described by Mukkamala et al as a novel spectral-domain optical coherence tomography (SD-OCT) finding of layered hyperreflective lines in the sub-retinal pigment epithelium (RPE) space, usually associated with chronic exudation from type 1 neovascularization (NV) in patients with age-related macular degeneration (AMD).[1] Typically associated with intense signal upon near-infrared reflectance scanning laser ophthalmoscopy (NIR-SLO), the Onion Sign was proposed by its discoverers to represent layers of precipitated lipid amidst chronic exudation[1, 2] after also considering collagen or fibrin.[1] Others authors suggested fibrovascular scarring,[3] mechanical strain on Bruch's membrane, and dystrophic calcification in drusen regression[4, 5] (Supplementary Table, available online) as possible histological correlates.

Independently Christakopoulous et al[6] hypothesized that hyperreflective lines in the Onion Sign represent cholesterol crystals, because they are transparent and not associated with shadowing, like calcification. This hypothesis is credible, because cholesterol crystals appear as linear, highly reflecting structures in atherosclerotic coronary artery plaques viewed by SD-OCT[7] in which reflections are generated from interfaces between crystal surfaces and surrounding tissue. This designation for cardiovascular disease was validated in autopsy and endarterial specimens analyzed by *ex vivo* OCT and subsequent histology[8, 9]. Tissue processing using ethanol dissolves crystals, leaving distinctive lucent clefts[10]. In human eye pathology, clefts have been reported within one disciform scar secondary to AMD[11] yet not in aged and early AMD eyes, which have cholesterol-rich lipoprotein deposits in drusen and Bruch's membrane[12].

Our goals are to document frequency and natural history of the Onion Sign in AMD patients and resolve the controversy behind the hyperreflective material with histology of two cases

identified among archival donor eyes by *ex vivo* SD-OCT. By confirming the cholesterol crystal hypothesis, our data reinforce the potential synergy of *in vivo* SD-OCT, *ex vivo* SD-OCT, and histology for molecular discovery. This information is valuable to clinicians as it aids in the understanding of pathophysiology underlying AMD as well as informing diagnosis and therapeutic decision-making.

Methods

The Western Institutional Review Board and the Institutional Review Board at UAB approved this retrospective, observational cohort study and experimental study, respectively. Research complied with the Health Insurance Portability and Accountability Act and adhered to the tenets of the Declaration of Helsinki.

Retrospective observational cohort study

Medical billing records from March 15, 2014 to September 15, 2014 were used to identify consecutive patients seen by a single physician (K.B.F) in a vitreoretinal referral practice located in New York, NY, with a diagnosis code 362.52 for nvAMD in the International Statistical Classification of Diseases and Related Health Problems, Ninth Revision (ICD-9). All patients had received anti-vascular endothelial growth factor (VEGF) therapy within the course of follow-up, although this was not an inclusion requirement. All patient medical charts, color fundus photography obtained with the Topcon Retinal Camera TRC 50DX (Topcon Corporation, Tokyo, Japan), SD-OCT and simultaneous NIR-SLO using a light stimulus of 815 nm obtained with the Spectralis (Heidelberg Engineering, Heidelberg, Germany) were reviewed. The Onion Sign was identified as the presence of layered, hyperreflective sub-RPE bands with SD-OCT imaging and correlated with findings on color fundus photography and NIR-SLO imaging. Serial eye-tracked SD-OCT scans were used to perform qualitative analysis of the Onion Sign from the time of first detection to the most recent visit. The SD-OCT scanning protocol used in all eyes comprised parallel horizontal line scans over the area of interest, each scan spaced approximately 150 to 250 μm apart, with automatic real-time (ART) averaging set between 16 to 32. The abundance of lines within the Onion Sign was taken as increased if the number or the lengths of hyperreflective lines increased, and decreased if numbers or lengths decreased.

To investigate the possibility of an association of the Onion Sign with systemic hypercholesterolemia, the use of an oral cholesterol-lowering medication was recorded. The association of medication use with the occurrence of the Onion Sign assessed for statistical significance using Fisher's exact test and SPSS software version 22.0 (IBM Corporation, New York, USA). A *p*-value of less than 0.05 was accepted as significant.

Histopathology study

Neovascular AMD eyes were identified through an *ex vivo* imaging screen of eyes accessioned for research purposes from non-diabetic white donors to the Alabama Eye Bank during the period 1996–2012. Median death-to-preservation time was 3:49 hours (range, 0:40–11:40 hours). Eyes were preserved by immersion in 1% paraformaldehyde and 2.5% glutaraldehyde in 0.1M phosphate buffer following anterior segment excision. Following

removal of vitreous, maculas were photographed in color on a stereomicroscope (SMZ-U, Nikon, Melville NY), using 35 mm color film (1996–2005) or a digital camera (CoolPix, Nikon; 2005–2009). For both image formats, pigmentary changes were accentuated with oblique trans-illumination via a dark-field base, and drusen were accentuated using epi-illumination via a ring light affixed to the objective of the dissecting scope. Eyes underwent additional multimodal *ex vivo* imaging including SD-OCT when prepared for histology (2011–2013). From each globe, an 8 mm diameter full-thickness tissue punch containing the fovea and temporal portion of the optic nerve head was removed with a trephine. This punch was held in a tissue holder (courtesy J. Fischer, Heidelberg Engineering) mounted on a Spectralis (Supplementary Figure 1, available online). The holder was a closed chamber with a 60-diopter lens in the front (facing into the SD-OCT instrument) and a slot to hold the tissue with the inner limiting membrane facing forward, in the back. Using tissues stabilized in this manner, we performed a 30°×20° SD-OCT volume (143 scans, 30 μm spacing, with ART set at 25) and red-free SLO. *Ex vivo* SD-OCT differs distinctly from its *in vivo* counterpart yet is interpretable with experience. Post-mortem edema overall reduces contrast in the neurosensory retina and underlying choroid[13]. The RPE-Bruch's membrane band is usually visible. The two synaptic layers, photoreceptor ellipsoid zone, and choroidal vessels are also visible in the best-preserved specimens. Fluid is hyporeflective. Eyes also underwent NIR-SLO and autofluorescence SLO with excitation wavelengths of 488 nm for lipofuscin-melanolipofuscin and 787 nm for melanosomes.

Macular tissue punches were post-fixed by osmium tannic acid paraphenylenediamine to accentuate extracellular lipid and embedded in epoxy resin (PolyBed 812, Polysciences, Warrington PA)[14]. Sub-micrometer-thick sections were stained with 1% toluidine blue, and reviewed and photodocumented with a 60× oil-immersion objective (numerical aperture = 1.4) and digital camera (XC10, Olympus; 1900× viewing magnification on a monitor). Histologic sections were annotated and uploaded to the Project MACULA online digital microscope (http://projectmacula). Forty eyes of 40 donors (25 women, 86.9 ± 5.9 years; 15 men, 82.2 ± 7.3 years) had nvAMD, defined by fibrovascular scarring in the presence of severe RPE change plus drusen and/or basal linear deposits (BLinD)[15]. Two nvAMD eyes exhibiting highly hyperreflective lines in the sub-RPE compartment consistent with the Onion Sign were identified. We use the nomenclature of Staurenghi et al[16] for SD-OCT bands and Zanzottera et al[17] for RPE morphology in histology.

Results

Clinical imaging and associations

A cohort of 230 eyes of 150 consecutive patients (mean age of 84 years, 108 women, 42 men) with nvAMD was identified. Of these, 16 eyes of 15 patients (7.0%; mean age of 82 years, 13 women, 2 men) were found to exhibit the Onion Sign with SD-OCT imaging. The Onion Sign corresponded to refractile yellow-gray exudates on color fundus photography and hyperreflective lesions on NIR-SLO imaging in all 16 eyes (Figure 1).

Qualitative analysis of serial SD-OCT scans revealed that the Onion Sign persisted in all 16 eyes over the follow-up duration (mean 3.7 years, range 0.5 – 5 years). Fluctuations in the appearance of the Onion Sign were noted, with 13 eyes exhibiting decreased abundance of

lines and 3 eyes showing increased abundance of lines over the follow up period. In addition, all 16 eyes with the Onion Sign were found to have adjacent areas of multiple intraretinal hyperreflective foci with SD-OCT imaging (Figure 2).

Of the 135 patients without the Onion Sign, 54 patients (40%) reported using oral cholesterol-lowering medication. This rate was consistent with the percentage of United States adults reporting use of these agents (39.1–54.4%[18]). Of the 15 patients with the Onion Sign, 11 patients (73%) were using cholesterol-lowering medications. This association was significant ($p<0.025$).

Histopathology

Of 40 donor eyes with histopathologic diagnosis of nvAMD, 2 eyes (5.0%) exhibited an Onion Sign on *ex vivo* SD-OCT imaging. *Ex vivo* SD-OCT and histology for **Case 1**, a 98-year-old white woman, are shown in Figure 3. Figures 3A,C show temporal to the foveal center a ~1.2 × 0.66 mm dome-shaped RPE elevation with a hyperreflective surface and an outwardly convex base. Figure 3A shows within the dome 3 groups of thin hyperreflective lines, radiating from a point on the temporal side, resembling a clinical Onion Sign. Histology in Figure 3B shows that the dome has 3 groups of linear clefts at angles corresponding exactly to the hyperreflective bands, surrounded by hemorrhage (abundant erythrocytes without formed vascular endothelium) and overlying an outwardly convex Bruch's membrane. Six additional Onion Signs were visible by *ex vivo* SD-OCT in this eye, including 2 more domes and 4 low flat elevations. All corresponded to reflective plaques visible in red-free SLO (not shown). In a dense fibrovascular scar with both subretinal and sub-RPE components were several lucent slits consistent with cholesterol clefts (not shown),[11] which had not been apparent by prior *ex vivo* imaging.

Figure 3C shows the RPE elevation of **Case 1** in a more inferiorly located B-scan, where it is associated with 3 hyperreflective foci within the neurosensory retina, each with distinct cellular content. Figure 3D shows Intraretinal RPE cells, which are irregularly shaped and packed with black spindle-shaped melanosomes and green-staining lipofuscin granules. Figure 3E,F shows cells with lipid droplets stained tan signifying lipid and few (Figure 3E) or absent (Figure 3F) RPE granules. Relative to the intraretinal RPE in Figure 3D, these tan-staining cells are larger and more spherical in shape, and they are clustered. We interpret cells in Figure 3E,F as phagocytes of monocyte origin that ingested and retained varying numbers of RPE granules while also differentiating into foam cells. Elsewhere in these sections are intraretinal fluid pockets and more hyperreflective foci (not shown).

Ex vivo multimodal imaging and histology for **Case 2**, a 91-year-old white man, are shown in Figures 4 and 5. Figure 4A is a color image showing a large, vertically elongated atrophic central area with punctate hyperpigmentation and ringed 270° by hyperpigmentation, representing an RPE detachment (PED). Within the central 0.7 mm, the PED is visible through the foveal floor as yellowish with punctate pigmentation, surrounded by golden hyperpigmentation with a sharp central border. Figure 4B shows that by 787 nm autofluorescence imaging, the PED is hypoautofluorescent with lobulated hyperautofluorescent borders. Figure 4C,D shows two *ex vivo* SD-OCT scans through the PED, which measured 3.720 × 2.583 mm (superior-inferior × nasal-temporal). Intraretinal

fluid pockets 1.38 mm and 0.69 mm in length were located temporal and nasal to the PED, respectively, and a 0.15 long mm-fluid pocket was present in the fovea (not shown). Increased light transmitted through the PED apex (Figure 4C,D) revealed numerous horizontal hyperreflective lines with scattered tiny hyperreflective spots against an inhomogeneous background reflectivity. One intense reflectivity source appeared as a thin line on SD-OCT and a plaque on NIR-SLO (not shown), suggesting a thin flat shape. The RPE band on the PED dome was irregular, with small hyperreflective spots between RPE and photoreceptors. In two locations on the PED dome (0.150 and 0.300 mm in length), the RPE band was thicker and associated with hyperreflective spots within the overlying neurosensory retina.

Histology for **Case 2** shows that the PED contains lucent linear clefts (Figures 4E and 5A, **#1**) cutting across several phases of fluid (Figure 5A, **#2–4**) that correspond to the hyperreflective lines and background reflectivity in SD-OCT, respectively. The fluid phases contain lipid, indicated by tan staining and contrast with clear plasma in choriocapillaries (Figure 5A, **arrow**; Figure 5A, **#2, #3**). Fluid from the PED and oily BLinD flanking the PED meet at a distinct phase boundary, emphasizing their different physical characteristics (Figure 5B, **arrow**). Judging from debris adhering to the PED under-surface (Figure 5B, **arrowheads**) and flocculent material within the PED (Figure 5A **#4**), the fluid may arise from within BLinD and dislodge pieces of this material. Within the PED fluid, macrophages with irregularly shaped cell bodies and inclusions that are large, deep brown, polydisperse, and unevenly packed account for the hyperreflective spots (Figure 4E). Sloughed RPE cells together with small areas of RPE atrophy on the PED apex account for the irregular pigmentation and 787 nm autofluorescence pattern in the *en face* view (Figure 4A–B). Intraretinal cysts containing tan-staining fluid with lipid droplets and cells shown in Figures 4F–I together account for the intraretinal hyporeflective cavities and hyperreflective spots, respectively. The cells have evenly-spaced spindle-shaped melanosomes and green-to-bronze staining lipofuscin granules consistent with Intraretinal RPE (Figure 4G,H) or polydisperse irregular inclusions consistent with phagocytes of monocyte origin (Figures 4F,I).

Discussion

To our knowledge, this study is the first to report frequency, natural history, and histological correlates of the Onion Sign in neovascular AMD. A long-lasting yet dynamic structure, the Onion Sign was visible in ~5–7% of nvAMD eyes and positively associated with intraretinal/ subretinal hyperreflective foci and intraretinal fluid. A possible association between the Onion Sign and systemic hypercholesterolemia was suggested by a significantly higher use of cholesterol-lowering medications in cases compared to controls. Histology of two cases with RPE elevation and sub-RPE hemorrhage/ fluid revealed that hyperreflective lines correlated with clefts created by the extraction of cholesterol crystals during tissue processing (**Supplementary Figure 6**, available online). Such crystals were reported in human eye pathology[11, 19] and in experimental hypercholesterolemia[20, 21] where birefringence before processing and clefts after processing can be directly demonstrated (**Supplementary Figure 6**; available online). Our data thus support the original hypotheses

that sub-RPE lipids are contributory[1] and that the contributing lipid has the chemical and physical form of crystalline cholesterol[6].

We believe that the histology cases from these clinically undocumented donors were nvAMD. Case 1 had disciform degeneration in the setting of basal laminar deposit and BLinD. Case 2 had a serous PED, intraretinal cysts, and hyperreflective spots in the same setting, yet a specific NV membrane was not found, likely due to the spacing of our standard section planes. For example, type 3 neovascularization is focal[22, 23] and could have been missed. However, the combination of a PED and intraretinal fluid in Case 2 merited consideration as nvAMD. Although histologic analysis used eyes different from those imaged clinically, attribution of hyperreflective lines to cholesterol clefts is justified, as follows: highly similar appearance of *ex vivo* and *in vivo* hyperreflective lines, distinctive appearance of cholesterol clefts, the clinically observed transmissivity characteristics[6], histologically validated imaging of crystals in cardiovascular disease, similar clinical and histologic prevalence in nvAMD eyes, and excellent preservation of donor eyes reducing probability of artifact. Because donor tissues were recovered prior to 2006, it can be concluded that the Onion Sign is not a consequence of anti-VEGF therapy, although we cannot exclude an effect of other treatments unknown to us. Eyes untreated by anti-VEGF therapy might be more likely to progress quickly to scars. The Onion Sign may develop preferentially in eyes with chronic exudation with absence of rapid neovascularization growth or hemorrhage from type 1 neovascularization. Chronic treatment with anti-VEGF agents in eyes showing some resistance and persistent leakage may predispose to this finding. Thus the similar frequency in a clinic population and treatment-naïve donors was somewhat surprising. Although we have not observed Onion Signs in non-nvAMD eyes in our clinical practice, others have[4] (Supplementary Table), making it premature to conclude that this sign localizes exclusively to neovascular disease. It is plausible that Onion Signs occur in serous PEDs and subclinical focal neovascularization indistinguishable by fluorescein or indocyanine green angiography. We restricted our current investigations to nvAMD.

Cholesterol crystal formation is important for atherosclerotic cardiovascular disease, forming early, instigating inflammation, and contributing to sudden cardiac events.[24] OCT imaging of coronary artery plaques yields curvilinear hyperreflective lines corresponding to histologically confirmed crystals.[7] Cholesterol has 2 chemical forms, unesterified (UC) and esterified (EC, bound to a fatty acid). It also has 3 physical forms that vary in proportions of UC, EC, and solubilizing phospholipid: droplets (EC, UC, phospholipid), membranes (UC, phospholipid), and crystals (UC only)[25]. Crystal formation in super-saturated solutions is affected by local physical factors, with cooler temperatures, lower pH, and higher saturation promoting formation[26], and degree of hydration affecting crystal shape (monohydrate, rhomboid plates; anhydrous, aciculate or needle-shaped)[27]. Our data suggest that appreciable lipid content in fluid (Case 2) and red blood cells (Case 1)[28] are potential contributors to UC super-saturation[24, 29].

It appears that super-saturation and subsequent crystal formation in PED requires an aqueous microenvironment that is distinct from the oily microenvironment of soft drusen and BLinD[30] (Figure 5). Drusen are extracellular lesions in the sub-RPE compartment that

provide a cleavage plane for invading neovessels[31]. The largest volumetric component of drusen is lipid especially EC, UC, and phosphatidylcholine, attributed to RPE-secreted apolipoprotein B, E-containing lipoproteins in a pathway driven by dietary lipid recycling in the outer retina[32]. Evidence for this model includes accumulation in Bruch's membrane throughout adulthood of solid particles with classic lipoprotein morphology containing cholesteryl esters rich in linoleate, RPE expression of hallmark lipoprotein secretion genes, secretion of apolipoprotein E-immunoreactive lipoprotein-like particles by highly-differentiated cultured RPE, and the inconsistent association of AMD at the person level with plasma lipoprotein levels[33]. Another cholesterol source contributing to sub-RPE super-saturation is also lipoproteins of systemic origin. The absence of cholesterol crystals from Bruch's membrane and drusen has been thought a crucial difference between AMD and systemic atherosclerosis, two diseases unified by early lipoprotein deposition in vessel walls[34].. Thus we propose that crystals represented by the Onion Sign have an important systemic contribution via plasma exudates, supported by the association with self-reported cholesterol-lowering medication. Although this retrospective study was limited by the lack of serum cholesterol data, this initial association between the Onion Sign and self-reported use of oral cholesterol-lowering medication can encourage future studies to investigate this relationship in detail. If our clinical findings are replicated, it may be possible that Onion Signs in AMD patients signify systemic hypercholesterolemia that should be monitored.

Sub-RPE cholesterol crystallization joins etiologically diverse retinal disorders with crystals, including Bietti crystalline dystrophy (CYP4V2 mutations)[19, 35] cerebrotendinous xanthomatosis (CYP27A1 mutations)[36], intraretinal crystals in macular telangiectasia type 2[37] and in AMD[2], pre-retinal crystals associated with triamcinolone usage[38], and refractile hydroxyapatite spherules in calcifying drusen.[39, 40] The Onion Sign is also distinct from other sub-RPE hyperreflective material such as fibrovascular scars with horizontal reflectivities caused by densely packed planes of collagen and fibroblasts. Other SD-OCT features with potential as crystalline are "plaques", single hyperreflective horizontal lines parallel to and very close to Bruch's membrane, described by Fleckenstein et al[41] and used as progression markers[42]. Yet cholesterol crystals in this location have not been illustrated by major AMD histological surveys.[12, 43–47] Whether these plaques are Onion precursors thus awaits further information.

Beyond showing cholesterol clefts, the histological cases provided unexpected insight into RPE fate over localized elevations of two different compositions (hemorrhage and fluid). For the first time, hyperreflective foci associated with intraretinal fluid in *ex vivo* SD-OCT were tracked to specific individual cells. Hyperreflective foci found in all 16 clinical cases are now plausibly also attributable to such cells. Recently we extensively surveyed RPE morphology in advanced AMD, also using high-resolution histology, to disclose characteristic RPE organelles and basal laminar deposit.[17] Two cellular phenotypes with a full complement of RPE granules that apparently form an anterior migratory pathway[17] were also present in our two cases. Many authors consider these cells macrophages or microglia[48–51]. In Case 1 some cells conferring hyperreflectivity are more readily attributable to cells of monocyte origin that phagocytized RPE, retaining telltale melanosomes, while also engorging with lipid droplets, like foam cells, which are

hyperreflective in coronary artery plaques[7]. Because we have not seen a resident population of non-pigmented cells in the subretinal space[52] of human donor eyes, we suggest that the lipid-filled cells are microglia that moved from inner to outer retina, as they do in degenerations and injuries[53]. Intriguingly, mouse microglia *in vitro* can take up 7-ketocholesterol, a pro-inflammatory oxysterol found in aging Bruch's membrane and drusen[54], and form intracellular lipid droplets[55]. It is tempting to speculate that microglia constitute one population of hyperreflective spots and anteriorly migrating RPE another. One way to test this hypothesis is to determine if cells are separable by size, clumping, motility, and characteristics in multimodal imaging studies[49, 56].

Although histology of a clinically characterized eye is considered a gold standard, our study notably identified a correlate to an *in vivo* SD-OCT imaging sign in an *ex vivo* SD-OCT screen of archived donor eyes. Limitations of this study include absence of crystal quantification in clinical and histological PED and molecular phenotyping of intraretinal hyperreflective cells. Nevertheless, data support the concept that SD-OCT is an essential tool for characterizing donor eyes in the pathology laboratory[57–59]. Targeting single cells of known reflectivity characteristics for labeling studies will be a powerful means to linking molecular discovery with contemporary clinical imaging. This capability is important, because the combination of comprehensive anatomic pathology and excellent clinical imaging is treasured in ophthalmology yet still a rarity[60], and laboratory animals lacking a macula do not yet faithfully replicate AMD.

Supplementary Material

Refer to Web version on PubMed Central for supplementary material.

Acknowledgments

We thank: personnel of the Alabama Eye Bank (Doyce V. Williams, Executive Director, and Alan S. Blake, Chief Technical Officer) for timely retrieval of donor eyes; Giovanni Staurenghi MD for facilitating the participation of author ECZ.

Financial support: Clinical research was supported by Macula Foundation and LuEsther T. Mertz Retinal Research Center. The Funding Organizations had no role in the design and conduct of this study. Histopathology was supported by the NIH grant R01 EY06109, and Research to Prevent Blindness, EyeSight Foundation of Alabama. Acquisition of donor eyes received additional support from International Retinal Research Foundation, National Eye Institute P30 EY003039, and the Arnold and Mabel Beckman Initiative for Macular Research. Creation of Project MACULA received additional support from the Edward N. and Della L. Thome Memorial Foundation and International Retinal Research Foundation

K. Bailey Freund M.D. is a consultant for Genentech, Optos, Heidelberg Engineering, Thrombogenics and Optovue.

Abbreviations

AMD	age-related macular degeneration
ART	automatic real-time averaging
BLinD	basal linear deposit
EC	esterified cholesterol

nIR	near infrared reflectance
NV	neovascularization
nvAMD	neovascular AMD
PED	retinal pigment epithelium detachment
RPE	retinal pigment epithelium
SD-OCT	spectral domain optical coherence tomography
SLO	scanning laser ophthalmoscope
UC	unesterified cholesterol
VEGF	vascular endothelial growth factor

Literature Cited

1. Mukkamala SK, Costa RA, Fung A, Sarraf D, Gallego-Pinazo R, Freund KB. Optical coherence tomographic imaging of sub-retinal pigment epithelium lipid. Arch Ophthalmol. 2012; 130:1–7. PMID 22892986.
2. Lima LH, Freund KB, Klancnik JM Jr, Spaide RF. Intraretinal crystalline deposits in neovascular age-related macular degeneration. Retina. 2010; 30:542–547. PMID 20084051. [PubMed: 20084051]
3. Coscas, G. Optical Coherence Tomography in Age-Related Macular Degeneration. Springer; 2009.
4. Querques G, Georges A, Ben Moussa N, Sterkers M, Souied EH. Appearance of regressing drusen on optical coherence tomography in age-related macular degeneration. Ophthalmology. 2014; 121:173–179. PMID 23891523. [PubMed: 23891523]
5. Bonnet C, Querques G, Zerbib J, et al. Hyperreflective pyramidal structures on optical coherence tomography in geographic atrophy areas. Retina. 2014; 34:1524–1530. PMID 24736463. [PubMed: 24736463]
6. Christakopoulos C, Pryds A, Larsen M. Subretinal lamellar bodies in polypoidal choroidal vasculopathy. Acta Ophthalmol. 2013; 91:e248–e249. PMID 23279931. [PubMed: 23279931]
7. Liu L, Gardecki JA, Nadkarni SK, et al. Imaging the subcellular structure of human coronary atherosclerosis using micro-optical coherence tomography. Nat Med. 2011; 17:1010–1014. PMID 21743452. [PubMed: 21743452]
8. Tearney GJ, Jang IK, Bouma BE. Optical coherence tomography for imaging the vulnerable plaque. J Biomed Opt. 2006; 11:021002. PMID 16674177. [PubMed: 16674177]
9. Yonetsu T, Bouma BE, Kato K, Fujimoto JG, Jang IK. Optical coherence tomography- 15 years in cardiology. Circ J. 2013; 77:1933–1940. PMID 23856651. [PubMed: 23856651]
10. Abela GS, Aziz K. Cholesterol crystals rupture biological membranes and human plaques during acute cardiovascular events--a novel insight into plaque rupture by scanning electron microscopy. Scanning. 2006; 28:1–10. PMID 16502619. [PubMed: 16502619]
11. Green WR, Key SN 3rd. Senile macular degeneration: a histopathologic study. Trans Am Ophthalmol Soc. 1977; 75:180–254. PMID 613523. [PubMed: 613523]
12. Curcio CA, Presley JB, Millican CL, Medeiros NE. Basal deposits and drusen in eyes with age-related maculopathy: evidence for solid lipid particles. Exp Eye Res. 2005; 80:761–775. PMID 15939032. [PubMed: 15939032]
13. Litts KM, Messinger JD, Dellatorre K, Yannuzzi LA, Freund KB, Curcio CA. Clinicopathological correlation of outer retinal tubulation in age-related macular degeneration. JAMA Ophthalmol. 2015 3/5/15 online. PMID 25742505.

14. Curcio CA, Messinger JD, Mitra AM, Sloan KR, McGwin G Jr, Spaide R. Human chorioretinal layer thicknesses measured using macula-wide high resolution histological sections. Invest. Ophthalmol. Vis. Sci. 2011; 52:3943–3954. PMID 21421869. [PubMed: 21421869]
15. Curcio CA, Medeiros NE, Millican CL. The Alabama age-related macular degeneration grading system for donor eyes. Invest. Ophthalmol. Vis. Sci. 1998; 39:1085–1096. PMID 9620067. [PubMed: 9620067]
16. Staurenghi G, Sadda S, Chakravarthy U, Spaide RF. Proposed lexicon for anatomic landmarks in normal posterior segment spectral-domain optical coherence tomography: The IN*OCT Consensus. Ophthalmology. 2014; 121:1572–1578. PMID 24755005. [PubMed: 24755005]
17. Zanzottera EC, Messinger JD, Ach T, Smith RT, Freund KB, Curcio CA. The Project MACULA retinal pigment epithelium grading system for histology and optical coherence tomography in age-related macular degeneration. Invest Ophthalmol Vis Sci. 2015 3/27/15 online. PMID 25813989.
18. Ford ES, Li C, Pearson WS, Zhao G, Mokdad AH. Trends in hypercholesterolemia, treatment and control among United States adults. Int J Cardiol. 2010; 140:226–235. PMID 19081646. [PubMed: 19081646]
19. Wilson DJ, Weleber RG, Klein ML, Welch RB, Green WR. Bietti's crystalline dystrophy. A clinicopathologic correlative study. Archives of Ophthalmology. 1989; 107:213–221. PMID 2783846. [PubMed: 2783846]
20. Ramírez AI, Salazar JJ, De Hoz R, et al. Macroglial and retinal changes in hypercholesterolemic rabbits after normalization of cholesterol levels. Exp Eye Res. 2006; 83:1423–1438. PMID 17007836. [PubMed: 17007836]
21. Salazar JJ, Ramírez AI, de Hoz R, et al. Alterations in the choroid in hypercholesterolemic rabbits: Reversibility after normalization of cholesterol levels. Exp Eye Res. 2006; 84:412–422. PMID 17178413. [PubMed: 17178413]
22. Monson DM, Smith JR, Klein ML, Wilson DJ. Clinicopathologic correlation of retinal angiomatous proliferation. Arch Ophthalmol. 2008; 126:1664–1668. PMID 19064845. [PubMed: 19064845]
23. Nagiel A, Sarraf D, Sadda SR, et al. Type 3 neovascularization: evolution, association with pigment epithelial detachment, and treatment response as revealed by spectral domain optical coherence tomography. Retina. 2015 PMID 25650713.
24. Abela GS. Cholesterol crystals piercing the arterial plaque and intima trigger local and systemic inflammation. J Clin Lipidol. 2010; 4:156–164. PMID 21122648. [PubMed: 21122648]
25. Small DM. George Lyman Duff memorial lecture. Progression and regression of atherosclerotic lesions. Insights from lipid physical biochemistry. Arteriosclerosis. 1988; 8:103–129. PMID 3348756. [PubMed: 3348756]
26. Vedre A, Pathak DR, Crimp M, Lum C, Koochesfahani M, Abela GS. Physical factors that trigger cholesterol crystallization leading to plaque rupture. Atherosclerosis. 2009; 203:89–96. PMID 18703195. [PubMed: 18703195]
27. Uskokovic V. Insights into morphological nature of precipitation of cholesterol. Steroids. 2008; 73:356–369. PMID 18215404. [PubMed: 18215404]
28. Virmani R, Kolodgie FD, Burke AP, et al. Atherosclerotic plaque progression and vulnerability to rupture: angiogenesis as a source of intraplaque hemorrhage. Arterioscler Thromb Vasc Biol. 2005; 25:2054–2061. PMID 16037567. [PubMed: 16037567]
29. Duewell P, Kono H, Rayner KJ, et al. NLRP3 inflammasomes are required for atherogenesis and activated by cholesterol crystals. Nature. 2010; 464:1357–1361. PMID 20428172. [PubMed: 20428172]
30. Curcio CA, Johnson M, Huang J-D, Rudolf M. Aging, age-related macular degeneration, and the Response-to-Retention of apolipoprotein B-containing lipoproteins. Prog Ret Eye Res. 2009; 28:393–422. PMID 19698799.
31. Killingsworth MC, Sarks JP, Sarks SH. Macrophages related to Bruch's membrane in age-related macular degeneration. Eye. 1990; 4:613–621. PMID 2226993. [PubMed: 2226993]
32. Curcio CA, Johnson M, Rudolf M, Huang J-D. The oil spill in ageing Bruch's membrane. Br J Ophthalmol. 2011; 95:1638–1645. PMID 21890786. [PubMed: 21890786]

33. Pikuleva I, Curcio CA. Cholesterol in the retina: the best is yet to come. Prog Ret Eye Res. 2014; 41:64–89. PMID 24704580.
34. Curcio CA, Johnson M, Huang J-D, Rudolf M. Apolipoprotein B-containing lipoproteins in retinal aging and age-related maculopathy. J. Lipid Res. 2010; 51:451–467. PMID 19797256. [PubMed: 19797256]
35. Pennesi ME, Weleber RG. High-resolution optical coherence tomography shows new aspects of Bietti crystalline retinopathy. Retina. 2010; 30:531–532. PMID 20139800. [PubMed: 20139800]
36. Dotti MT, Rufa A, Federico A. Cerebrotendinous xanthomatosis: heterogeneity of clinical phenotype with evidence of previously undescribed ophthalmological findings. J Inherit Metab Dis. 2001; 24:696–706. PMID 11804206. [PubMed: 11804206]
37. Sallo FB, Leung I, Chung M, et al. Retinal crystals in type 2 idiopathic macular telangiectasia. Ophthalmology. 2011; 118:2461–2467. PMID 21839520. [PubMed: 21839520]
38. Sarraf D, Vyas N, Jain A, et al. Triamcinolone-associated crystalline maculopathy. Arch Ophthalmol. 2010; 128:685–690. PMID 20547944. [PubMed: 20547944]
39. Suzuki M, Curcio CA, Mullins RF, Spaide RF. REFRACTILE DRUSEN: Clinical Imaging and Candidate Histology. Retina. 2015; 35:859–865. PMID 25768253. [PubMed: 25768253]
40. Thompson RB, Reffatto V, Bundy JG, et al. Identification of hydroxyapatite spherules provides new insight into subretinal pigment epithelial deposit formation in the aging eye. Proc Natl Acad Sci U S A. 2015; 112:1565–1570. PMID 25605911. [PubMed: 25605911]
41. Fleckenstein M, Charbel Issa P, Helb HM, et al. High-resolution spectral domain-OCT imaging in geographic atrophy associated with age-related macular degeneration. Invest Ophthalmol Vis Sci. 2008; 49:4137–4144. PMID 18487363. [PubMed: 18487363]
42. Moussa K, Lee JY, Stinnett SS, Jaffe GJ. Spectral domain optical coherence tomography-determined morphologic predictors of age-related macular degeneration-associated geographic atrophy progression. Retina. 2013; 33:1590–1599. PMID 23538573. [PubMed: 23538573]
43. Sarks SH. Ageing and degeneration in the macular region: a clinico-pathological study. Br. J. Ophthalmol. 1976; 60:324–341. PMID 952802. [PubMed: 952802]
44. van der Schaft TL, Mooy CM, de Bruijn WC, Oron FG, Mulder PGH, de Jong PTVM. Histologic features of the early stages of age-related macular degeneration. Ophthalmol. 1992; 99:278–286. PMID 1553220.
45. Green WR, Enger C. Age-related macular degeneration histopathologic studies: the 1992 Lorenz. E. Zimmerman Lecture. Ophthalmology. 1993; 100:1519–1535. PMID 7692366. [PubMed: 7692366]
46. Sarks S, Cherepanoff S, Killingsworth M, Sarks J. Relationship of basal laminar deposit and membranous debris to the clinical presentation of early age-related macular degeneration. Invest Ophthalmol Vis Sci. 2007; 48:968–977. PMID 17325134. [PubMed: 17325134]
47. Curcio CA, Messinger JD, Sloan KR, McGwin G Jr, Medeiros NE, Spaide RF. Subretinal drusenoid deposits in non-neovascular age-related macular degeneration: morphology, prevalence, topography, and biogenesis model. Retina. 2013; 33:265–276. PMID 23266879. [PubMed: 23266879]
48. Buschini E, Piras A, Nuzzi R, Vercelli A. Age related macular degeneration and drusen: neuroinflammation in the retina. Progress in neurobiology. 2011; 95:14–25. PMID 21740956. [PubMed: 21740956]
49. Gocho K, Sarda V, Falah S, et al. Adaptive optics imaging of geographic atrophy. Invest Ophthalmol Vis Sci. 2013; 54:3673–3680. PMID 23620431. [PubMed: 23620431]
50. Leuschen JN, Schuman SG, Winter KP, et al. Spectral-domain optical coherence tomography characteristics of intermediate age-related macular degeneration. Ophthalmology. 2013; 120:140–150. PMID 22968145. [PubMed: 22968145]
51. Coscas G, De Benedetto U, Coscas F, et al. Hyperreflective dots: a new spectral-domain optical coherence tomography entity for follow-up and prognosis in exudative age-related macular degeneration. Ophthalmologica. 2013; 229:32–37. PMID 23006969. [PubMed: 23006969]
52. Xu H, Chen M, Manivannan A, Lois N, Forrester JV. Age-dependent accumulation of lipofuscin in perivascular and subretinal microglia in experimental mice. Aging Cell. 2008; 7:58–68. PMID 17988243. [PubMed: 17988243]

53. Karlstetter M, Scholz R, Rutar M, Wong WT, Provis JM, Langmann T. Retinal microglia: Just bystander or target for therapy? Prog Retin Eye Res. 2014 PMID 25476242.

54. Rodriguez IR, Clark ME, Lee JW, Curcio CA. 7-ketocholesterol accumulates in ocular tissues as a consequence of aging and is present in high levels in drusen. Exp Eye Res. 2014; 128:151–155. PMID 25261634. [PubMed: 25261634]

55. Indaram M, Ma W, Zhao L, Fariss RN, Rodriguez IR, Wong WT. 7-ketocholesterol increases retinal microglial migration, activation, and angiogenicity: a potential pathogenic mechanism underlying age-related macular degeneration. Sci Rep. 2015; 5:9144. PMID 25775051. [PubMed: 25775051]

56. Lammer J, Bolz M, Baumann B, et al. Detection and analysis of hard exudates by polarization-sensitive optical coherence tomography in patients with diabetic maculopathy. Invest Ophthalmol Vis Sci. 2014; 55:1564–1571. PMID 24526446. [PubMed: 24526446]

57. Ghazi NG, Dibernardo C, Ying H, Mori K, Gehlbach PL. Optical coherence tomography of peripheral retinal lesions in enucleated human eye specimens with histologic correlation. Am J Ophthalmol. 2006; 141:740–742. PMID 16564813. [PubMed: 16564813]

58. Brown NH, Koreishi AF, McCall M, Izatt JA, Rickman CB, Toth CA. Developing SDOCT to assess donor human eyes prior to tissue sectioning for research. Graefes Arch Clin Exp Ophthalmol. 2009; 247:1069–1080. PMID 19225801. [PubMed: 19225801]

59. Bagheri N, Bell BA, Bonilha VL, Hollyfield JG. Imaging human postmortem eyes with SLO and OCT. Advances in experimental medicine and biology. 2012; 723:479–488. PMID 22183367. [PubMed: 22183367]

60. Klein ML, Wilson DJ. Clinicopathologic correlation of choroidal and retinal neovascular lesions in age-related macular degeneration. American Journal of Ophthalmology. 2011; 151:161–169. PMID 20970772. [PubMed: 20970772]

61. Friedman E, Smith TR. Clinical and pathological study of choroidal lipid globules. Arch Ophthalmol. 1966; 75:334–336. PMID 5903818. [PubMed: 5903818]

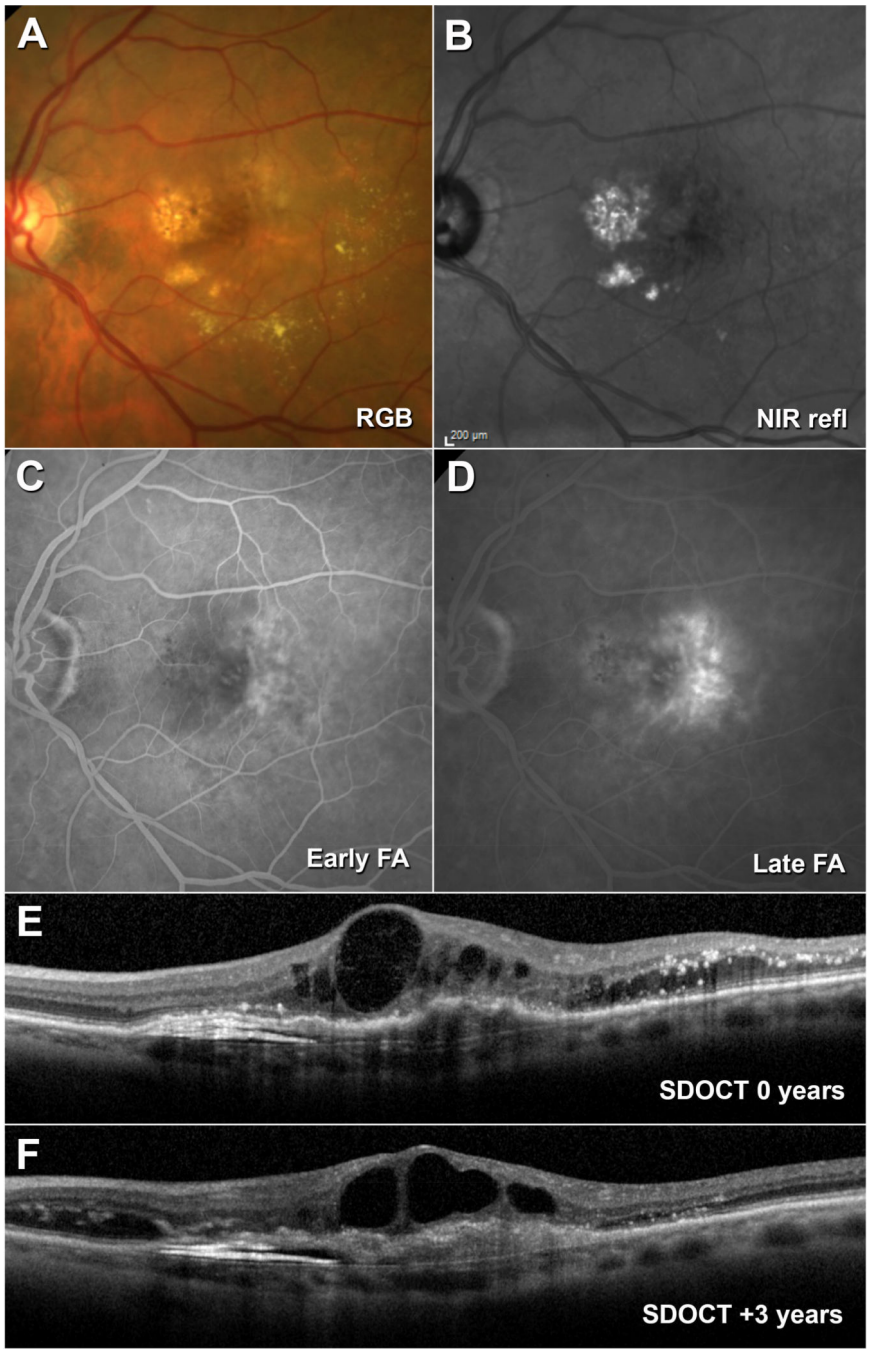

Figure 1. Multimodal imaging of the Onion Sign in neovascular age-related macular degeneration

A 72-year-old white woman with exudative changes. **A.** Color fundus photograph (RGB) shows yellow-gray exudation just nasal to the fovea and circinate yellow exudates. **B.** NIR-SLO (NIR-refl) shows hyperreflectivity of the yellow-gray exudates nasal to the fovea. **C.** Early fluorescein angiogram showing hyperfluorescence temporal to the fovea consistent with neovascularization. **D.** Late fluorescein angiogram showing late leakage, also consistent with neovascularization, but not co-localizing with the Onion Sign. **E.** SD-OCT

scan through the fovea showing the Onion Sign nasal to the fovea, consisting of multiple layered hyperreflective lines below the RPE. There are multiple intraretinal hyperreflective foci temporal to the fovea. **F.** SD-OCT scan through the fovea 3 years later shows persistence of the Onion Sign, with fewer hyperreflective lines.

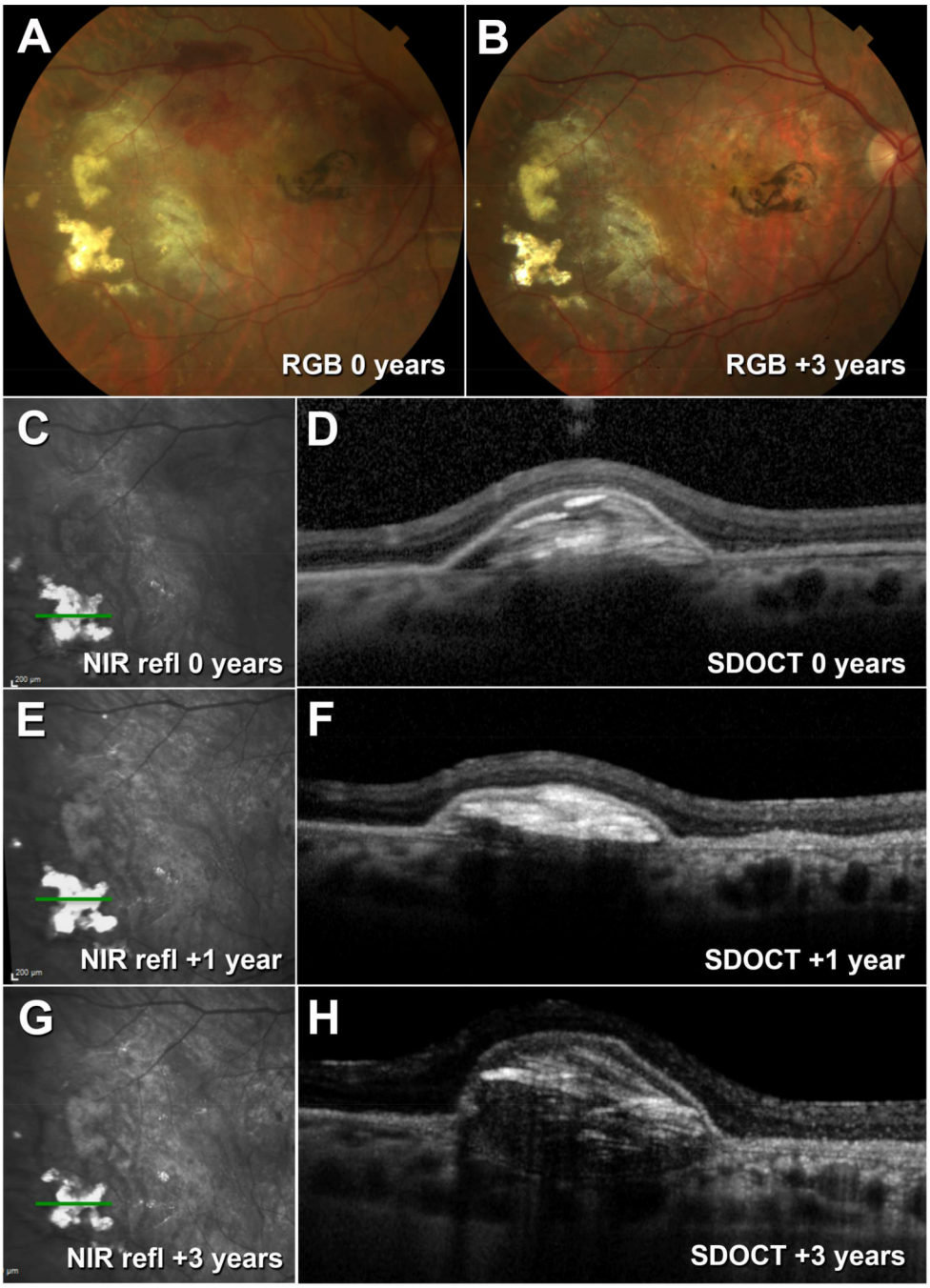

Figure 2. The Onion Sign in neovascular age-related macular degeneration fluctuates in size and complexity

A 67-year-old white woman with exudative macular changes. **A.** Color fundus photography (RGB) shows refractile yellow exudation temporal to the macula which occurred while receiving intravitreal ranibizumab injections. **B.** Color fundus photograph taken 3 years later shows the same refractile yellow exudation. **C,D.** NIR-SLO (NIR refl) and SD-OCT performed at this visit show that the hyperreflective lesion on NIR-SLO corresponds to an Onion Sign consisting of multiple layered hyperreflective lines below elevated RPE. **E,F.**

Corresponding NIR-SLO and SD-OCT taken 1 year later show persistence of the Onion Sign, with reduced dome height and fewer clearly discernable hyperreflective lines. **G,H.** NIR-SLO and SD-OCT through the refractile exudates taken 3 years later show persistence of the Onion Sign, with increased dome height and more hyperreflective lines.

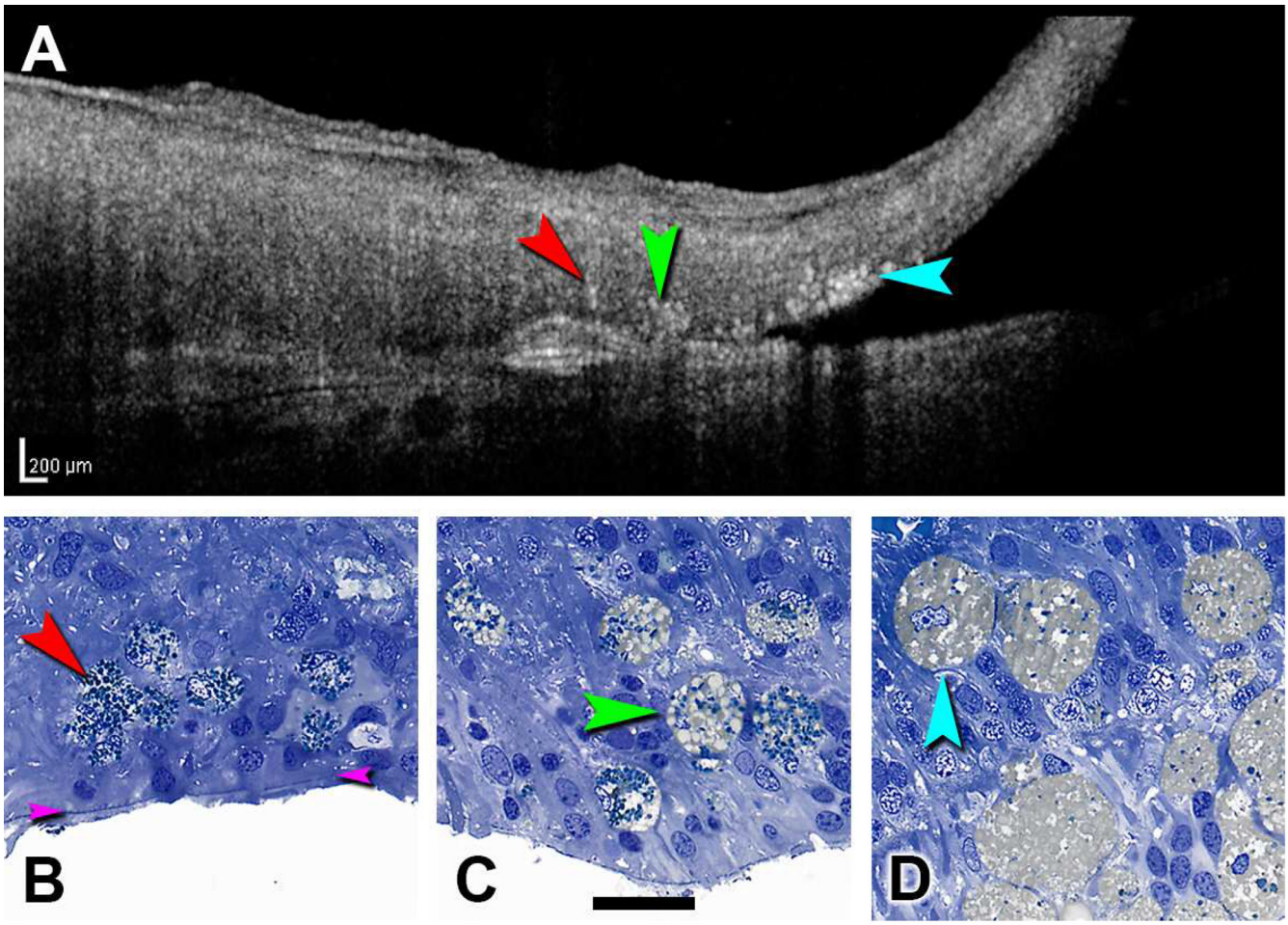

Figure 3. ***Ex vivo*** **SD-OCT and histology of the Onion Sign**

Sub-micrometer epoxy section, toluidine blue; 98-year-old white woman with neovascular AMD. **A.** *Ex vivo* SD-OCT shows 3 groups of thin highly hyperreflective lines (arrowheads) within an overall hyperreflective RPE elevation. The foveal center is nasal to the elevation (off the left edge). **B.** Histology reveals cholesterol clefts clustered in 3 planes corresponding to the hyperreflective lines in panel A (arrowheads). Bruch's membrane (black arrowheads) is bowed outward. RPE, retinal pigment epithelium; asterisk, basal laminar deposit; Ch, choroid; Sc, sclera; g, Friedman lipid globule[61]. Bar, 100 µm. **C.** *Ex vivo* SD-OCT through the same elevation at a location inferior to A shows 3 hyperreflective foci in the neurosensory retina that are magnified in D (red), E (green), and F (teal). Bar in E, 25 µm, applies to D–F. **D–F.** Intraretinal RPE has full complement of black spindle-shaped melanosomes and green-staining lipofuscin granules (**D**). Cells of presumed monocyte origin with tan-staining lipid droplets and sparse (**E**) or absent (**F**) RPE melanosomes.

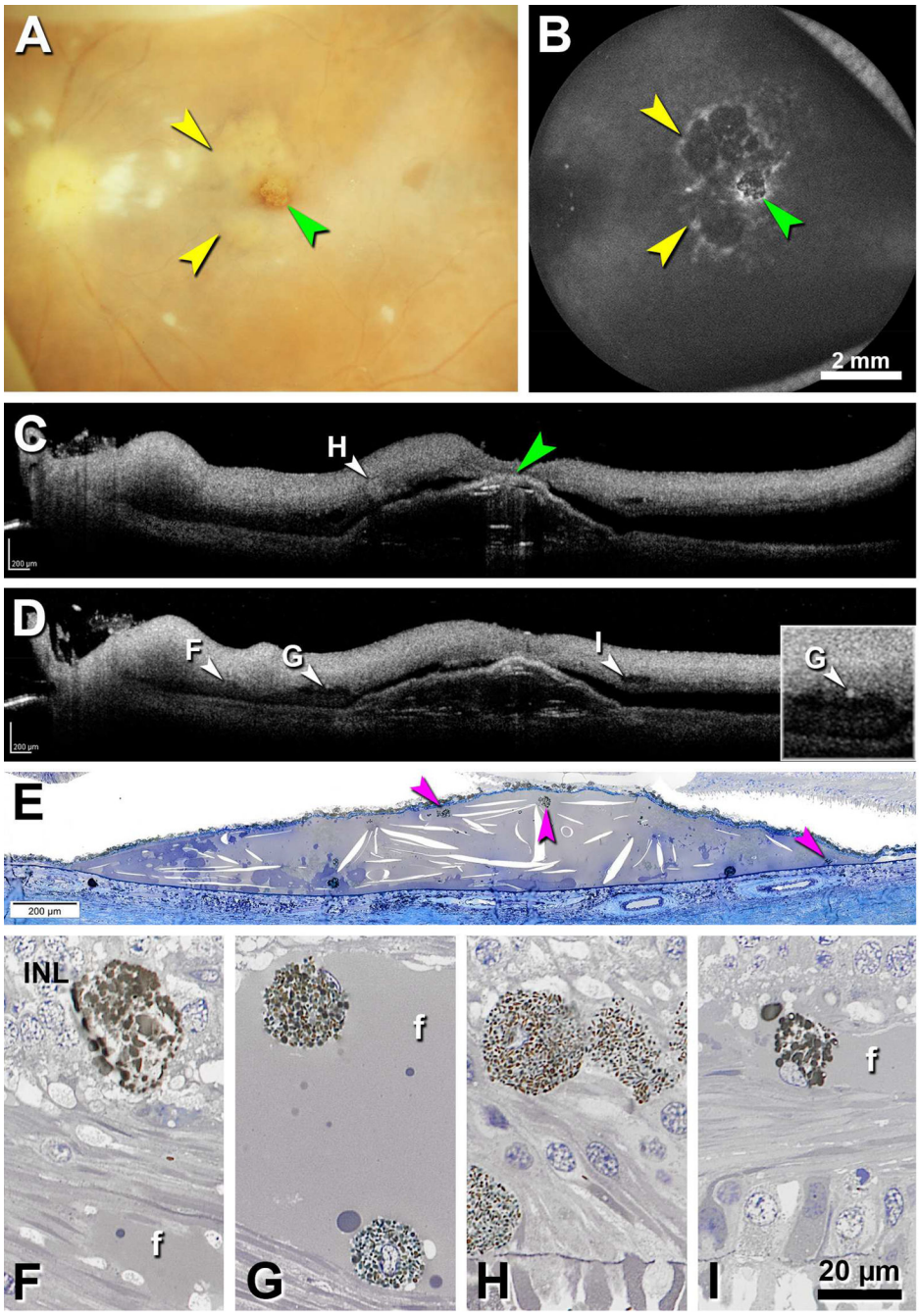

Figure 4. ***Ex vivo*** **imaging and histology of an RPE detachment (PED) with an Onion Sign and associated hyperreflective foci**

Sub-micrometer epoxy section, toluidine blue; 91-year-old white man with neovascular AMD. **A.** Color photography shows RPE atrophy (yellow) with a central PED (green). Cotton wool spots (white clumps between the PED and the optic nerve head) are visible in color and NIR-SLO (not shown); they are not visible in 787 nm autofluorescence (panel B). **B.** 787 nm autofluorescence shows that the PED (green) is hypo-autofluorescent with a hyper-autofluorescent border (yellow). **C, D.** SD-OCT scans through (**C**) and inferior (**D**) to

the foveal center show horizontal hyperreflective lines within the PED (green). Median length of clefts is 105.1 μm, range 39.9–533.9 μm. Hyperreflective foci F–I are magnified in panels F–I. **E.** The PED contains numerous lucent needle-shaped clefts that are cholesterol crystals extracted by histological processing. Cells in the fluid (pink) are presumed macrophages. **F–I.** Presumed macrophages have polydisperse irregular inclusions. Intraretinal RPE have spindle-shaped melanosomes and monodisperse green-stained lipofuscin. Fluid (f). Black arrows, ELM. Insert G was brightened to highlight a hyperreflective spot believed to represent one or several cells.

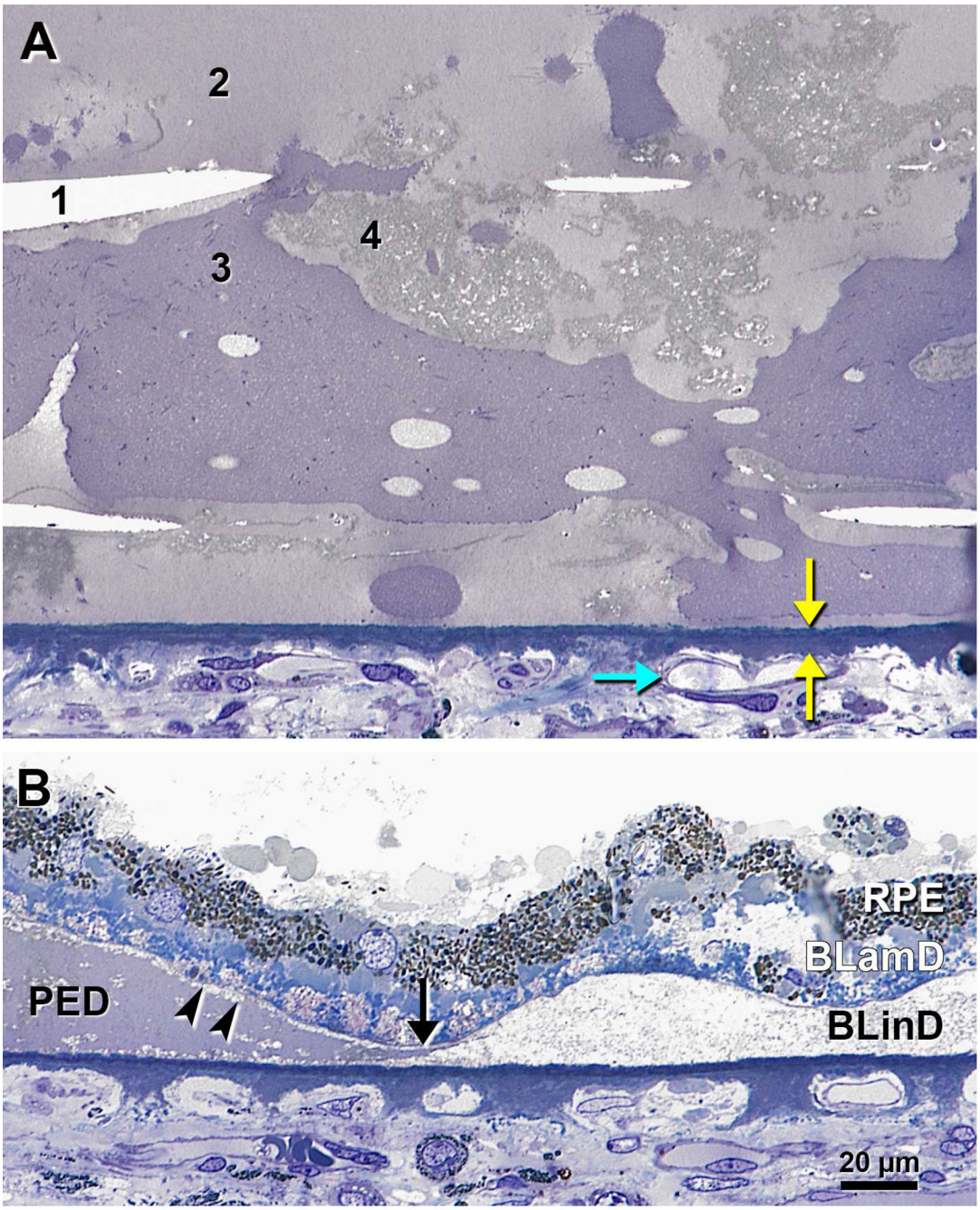

Figure 5. Contents and microenvironment of a large PED with an Onion Sign

Same eye as Figure 4. **A.** Cholesterol clefts (1), and three fluid phases containing lipid. (2–4); #4 denotes flocculent material apparently originating from lipoprotein-derived debris in adjoining basal linear deposit (BLinD). Teal arrow, choriocapillary with clear plasma. Yellow arrows, Bruch's membrane. **B.** At the margin of the Onion Sign-bearing PED, fluid meets oily BLinD at a phase boundary (black arrow). Debris adheres to the PED under-surface (black arrowheads). BLamD, basal laminar deposit. Bar, 20 µm.